An elementary quantum network of entangled optical atomic clocks

B. C. Nichol*, R. Srinivas*, D. P. Nadlinger, P. Drmota, D. Main, G. Araneda, C. J. Ballance, and D. M. Lucas
Department of Physics, University of Oxford, Clarendon Laboratory, Parks Road, Oxford OX1 3PU, U.K.
(Dated: 14/11/2022)

Optical atomic clocks are our most precise tools to measure time and frequency[1–3]. Precision frequency comparisons between clocks in separate locations enable one to probe the space-time variation of fundamental constants[4,5] and the properties of dark matter[6,7], to perform geodesy[8–10], and to evaluate systematic clock shifts. Measurements on independent systems are limited by the standard quantum limit (SQL); measurements on entangled systems can surpass the SQL to reach the ultimate precision allowed by quantum theory — the Heisenberg limit. While local entangling operations have demonstrated this enhancement at microscopic distances[11–16], comparisons between remote atomic clocks require the rapid generation of high-fidelity entanglement between systems that have no intrinsic interactions. Using a photonic link[17,18] we entangle two $^{88}Sr^{+}$ ions separated by a macroscopic distance[19] ($\approx$2 m), to demonstrate the first quantum network of entangled optical clocks. For frequency comparisons between the ions, we find that entanglement reduces the measurement uncertainty by nearly $\sqrt{2}$, the value predicted for the Heisenberg limit. Today's optical clocks are typically limited by dephasing of the probe laser[20]; in this regime, we find that entanglement yields a factor 2 reduction in the measurement uncertainty compared to conventional correlation spectroscopy techniques[20–22]. We demonstrate this enhancement for the measurement of a frequency shift applied to one of the clocks. This two-node network could be extended to additional nodes[23], to other species of trapped particles, or – via local operations – to larger entangled systems.

Nonclassical states enable measurement precision beyond the standard quantum limit (SQL)[24–27]. For example, quantum-enhanced measurements have been used for gravitational wave sensing[28,29], searches for dark matter[30], force sensing[31,32], measurements of quadrupole moments[13], local Lorentz invariance[14], and atomic isotope shifts[15]. While quantum networks[33] have been used for quantum cryptography[34], quantum computation[35], and verifications of quantum theory[36], they could potentially be used for enhanced metrology by distributing entanglement between remote systems. This enhancement is particularly important for optical atomic clock comparisons, where the number of measurements required to reach the noise floor is presently limited by the single-shot measurement uncertainty set by the SQL. Harnessing entanglement to move beyond the SQL and reach precision floors faster will enable the detection of phenomena on shorter timescales, and reveal previously undetectable signals by reducing the demands on the stability of the system.

The standard method for optical atomic clock comparisons requires the measurement of each atomic frequency relative to a laser. This laser is used to drive a narrow optical atomic transition and its relative frequency is determined by observing changes in the atomic state. This measurement is typically performed using a Ramsey experiment[37,38], where a superposition of two states, $|\downarrow\rangle$ and $|\uparrow\rangle$, evolves for a duration T_R in between two $\pi/2$ pulses. A difference frequency between the atom and the laser results in a relative phase between the two atomic states, which can be measured by repeated observations of the final state of the atom. For a single atom i, the expectation value of this measurement is

$$\langle\hat{\Pi}_i\rangle = C_i\cos(\Delta_i T_R+\phi_i), \tag{1}$$

where $\Delta_i=\omega_L-\omega_i$ is the detuning between the laser frequency, ω_L, and the atomic resonance frequency, ω_i. Here, ϕ_i is the phase of the second $\pi/2$ pulse with respect to the first pulse, C_i is the signal contrast, which is ideally 1 in the absence of decoherence, and $\hat{\Pi}_i=\hat{\sigma}_{zi}=|\uparrow\rangle\langle\uparrow|-|\downarrow\rangle\langle\downarrow|$ is the spin measurement operator. The corresponding uncertainty in the frequency Δ_i for a single quantum measurement is

$$\delta\Delta_i=\frac{\delta\langle\hat{\Pi}_i\rangle}{C_i T_R}, \tag{2}$$

where $\delta\langle\hat{\Pi}_i\rangle$ is ideally limited by quantum projection noise[39]. Minimising this 'single-shot' uncertainty minimises the number of measurements required to reach a given precision. To compare two clocks, we wish to measure the frequency difference, $\Delta_-=\Delta_1-\Delta_2=\omega_2-\omega_1$. For completely independent systems, separate measurements of Δ_1 and Δ_2 are required. Assuming each measurement has the same uncertainty, the single-shot uncertainty of Δ_- is $\delta\Delta_{-,s}=\sqrt{2}\delta\Delta_i$. A direct measurement of Δ_- can be made by probing two atoms with simultaneous Ramsey experiments and measuring the correlated two-ion parity signal[12]

$$\langle\hat{\Pi}\rangle = P_+\cos(\Delta_+T_R+\phi_+)+P_-\cos(\Delta_-T_R+\phi_-), \tag{3}$$

where $\Delta_\pm=\Delta_1\pm\Delta_2$, $\phi_\pm=\phi_1\pm\phi_2$, and $\hat{\Pi}=\hat{\sigma}_{z1}\hat{\sigma}_{z2}$. The probabilities of the two-atom state during the Ramsey delay being $\frac{1}{\sqrt{2}}(|\downarrow\uparrow\rangle+e^{i\phi}|\uparrow\downarrow\rangle)$ or $\frac{1}{\sqrt{2}}(|\downarrow\downarrow\rangle+e^{i\phi'}|\uparrow\uparrow\rangle)$ are given by P_- and P_+ respectively, where ϕ and ϕ' are arbitrary phases. For two maximally-entangled atoms, we can set $P_-=1$ (and $P_+=$

*These authors contributed equally.
Email:bethan.nichol@physics.ox.ac.uk,
raghavendra.srinivas@physics.ox.ac.uk

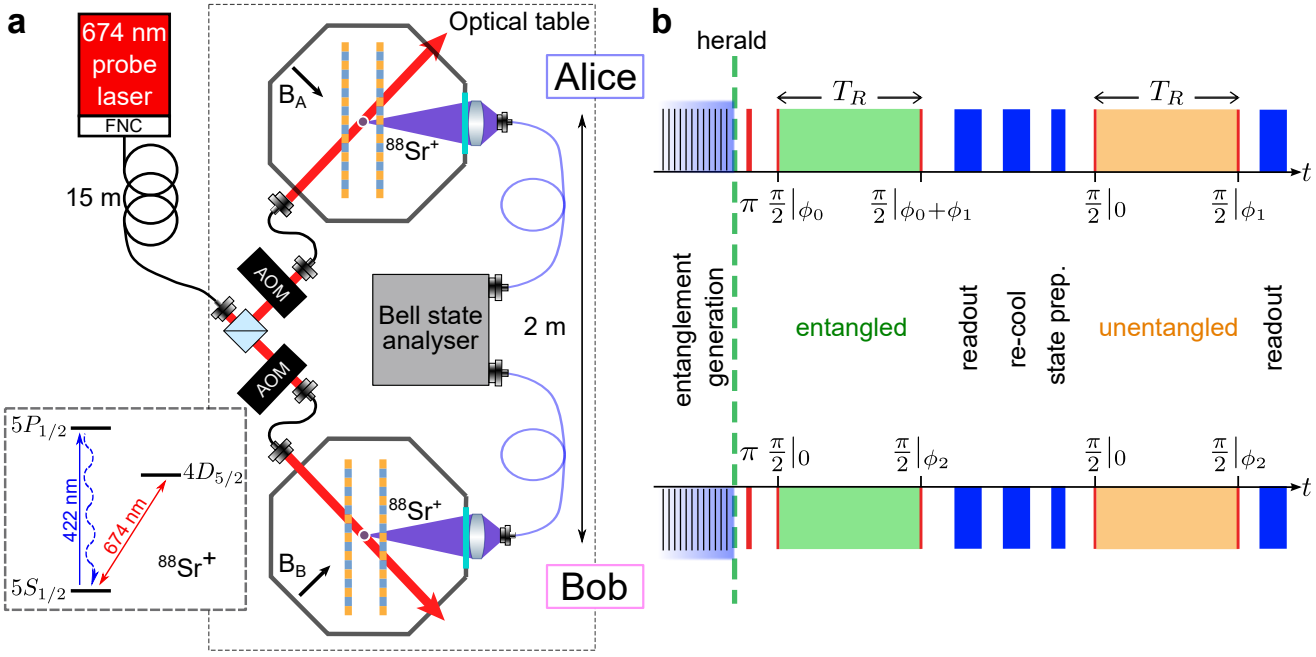

FIG. 1: **Network of entangled optical clocks. a**, Experimental apparatus. The network comprises two trapped-ion systems, Alice and Bob, separated by 2 m, each containing a single $^{88}Sr^+$ ion (not to scale). We use a photonic link to generate remote entanglement; spontaneously emitted 422 nm photons are transmitted via optical fibres to a Bell state analyser where a measurement projects the ions into an entangled state within the $S_{1/2}$ manifold. We map this entanglement to the $S_{1/2} \leftrightarrow D_{5/2}$ optical clock transition using a common 674 nm laser, which has fibre-noise cancellation (FNC) from the laser system to the optical table. This laser is also used to probe the clock transition. Each trap has an independent acousto-optical modulator (AOM) for switching, frequency and phase control. A magnetic field of ~ 0.5 mT, indicated by $B_{A|B}$, provides a quantisation axis in each trap. The relevant energy levels of $^{88}Sr^+$ are shown in the inset. **b**, Experimental pulse sequence. In a single experimental sequence, we measure the ion states after Ramsey experiments on both the entangled and unentangled states. Entanglement generation, using simultaneous 422 nm excitation pulses, is repeatedly attempted until a coincident two-photon detection at the Bell state analyser heralds entanglement. A 674 nm π-pulse maps the entanglement to the optical clock transition. We then simultaneously perform a Ramsey experiment on each ion with a total probe duration of T_R; spin-echo pulses during T_R are not shown. The phase of the first $\pi/2$ pulse on Alice is $\phi_0 = \phi + \pi$, where ϕ is the phase of the initial entangled state. Following ion readout, cooling, and state preparation, this process is repeated for the unentangled state.

0) to measure Δ_- directly with maximum signal contrast, resulting in a single-shot uncertainty $\delta\Delta_{-,e} = \delta\Delta_i = \delta\Delta_{-,s}/\sqrt{2}$. This uncertainty is $\sqrt{2}$ lower than the uncertainty achieved with two independent atoms, following the expected Heisenberg scaling [40].

With present optical clock technology, dephasing of the probe laser typically limits the uncertainty that can be achieved[41,42]. For the single-atom measurements, laser phase noise effectively randomises ϕ_i in Eq. 1, reducing the contrast C_i and setting a practical limit on the duration T_R. In this regime, entanglement offers an additional advantage as ϕ_- has complete cancellation of common phase fluctuations and is only affected by differential phase noise between the two systems. If entanglement is not available as a resource, this insensitivity can also be accessed by using conventional correlation spectroscopy[43–46], which involves simultaneous measurements with a common probe laser and an unentangled two-atom state[21], as recently demonstrated by Clements *et al.*[20] for two macroscopically-separated clocks. However, in this scenario $P_+ = P_- = \frac{1}{2}$ which sets the limit on the measurement uncertainty to $\delta\Delta_{-,u} = 2\delta\Delta_i = \sqrt{2}\delta\Delta_{-,s}$, a factor of $\sqrt{2}$ worse than independent single-ion measurements. Entanglement enables one to combine this noise-insensitivity with the maximum measurement precision allowed by quantum mechanics.

The challenge in realising this entanglement enhancement for remotely-located atoms is that the entangled state needs to be generated with both high fidelity (to achieve $P_- \approx 1$) and high speed (to maximise the measurement duty cycle). This has prevented previous experimental demonstrations. Using our two-node trapped-ion quantum network[19], we can create entangled states of two remote $^{88}Sr^+$ ions with a fidelity of 0.960(2) in an average duration of 8 ms[47], sufficient to realise the first elementary network of entangled optical clocks. We compare atom-atom frequency difference measurements of the $^{88}Sr^+$ optical clock transition frequency using (i) independent measurements on each atom, and correlated measurements of both (ii) unentangled atoms, and (iii) entangled atoms. We characterise the enhancement gained from entanglement and, as a proof-of-principle, make an entanglement-

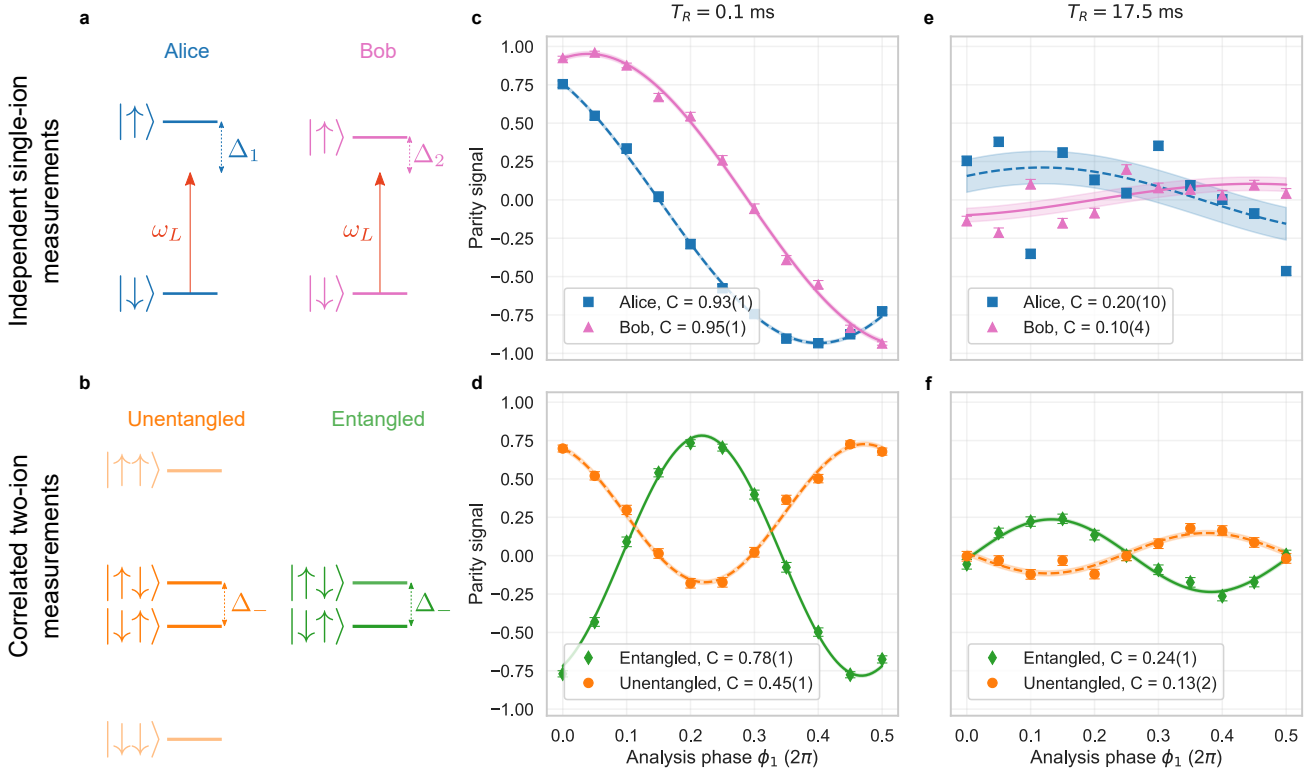

FIG. 2: **Spectroscopy with and without entanglement. a**, We perform Ramsey experiments on Alice's (blue) and Bob's (pink) atoms, using a probe laser with frequency ω_L. These experiments can measure the atoms' detunings Δ_1 and Δ_2 between ω_L and the $|\downarrow\rangle \leftrightarrow |\uparrow\rangle$ transitions. Thus, two independent measurements are required to obtain the difference frequency $\Delta_- = \Delta_1 - \Delta_2$. **b**, With entanglement, only a single measurement is required for Δ_- using the two-atom states $|\downarrow\uparrow\rangle$ and $|\uparrow\downarrow\rangle$. A single measurement can also be performed using unentangled states, at the cost of having population in the additional states $|\downarrow\downarrow\rangle$ and $|\uparrow\uparrow\rangle$ that does not contribute to the signal. For **c**-**f**, we scan the analysis phase $\phi_1 = -\phi_2$ from 0 to π radians. We plot the single-ion **(c)** and two-ion parity **(d)** signals at a Ramsey duration of 0.1 ms. Imperfect entangled-state generation and an increased effect from the imperfect spin-echo pulses reduce the contrast of the entangled state (green diamonds), compared to the single ion scans (blue squares and pink triangles). The two-ion signal from the unentangled state (orange circles) has about half the contrast of the entangled state signal; the y-offset from 0 arises from the term containing Δ_+ in Eq. 3. Similarly, we plot the single-ion **(e)** and two-ion parity **(f)** signals at a Ramsey duration of 17.5 ms, by which point the y-offset from the Δ_+ term has averaged to zero (see Supplementary Information § J) . At this duration, both the single-ion and two-ion signals are reduced due to qubit decoherence from differential magnetic field fluctuations, but the entanglement enhancement is still evident. The single-ion signals have almost no visibility and increased uncertainty in the fits due to sensitivity to common-mode laser phase noise. Experimental data are shown as points, with error bars calculated from projection noise. Fits to the data (lines), and their corresponding contrasts C, are shown with 68% confidence intervals (shaded region), following Eq. 1 and Eq. 3 for the single-ion and two-ion signals respectively.

enhanced measurement of a frequency shift applied to one of the atoms.

For these experiments, we drive the $5S_{1/2} \leftrightarrow 4D_{5/2}$ optical clock transition in each trapped-ion system (labelled Alice and Bob) with light from a common 674 nm laser, as shown in Fig. 1a. Entanglement generation, Doppler cooling, state preparation, and readout are performed using the 422 nm $S_{1/2} \rightarrow P_{1/2}$ transition. The initial atom-atom entanglement is generated using qubit states within the $S_{1/2}$ manifold that are separated at radiofrequency by 14 MHz[19]. To map this entanglement to the 445 THz optical qubit in each atom, we use a resonant 674 nm π-pulse on the $S_{1/2} \leftrightarrow D_{5/2}$ transition (see Supplementary Information § A). We create the entangled state $|\Psi\rangle = \frac{1}{\sqrt{2}}(|\downarrow\uparrow\rangle \pm e^{i\phi}|\uparrow\downarrow\rangle)$, where ϕ is set by the difference in optical paths and magnetic field strengths between the two systems, and $\pm$ depends on the measurement outcome of the Bell state analyser[48]. The qubit states are $|\downarrow\rangle \equiv |S_{1/2}, m_j = -1/2\rangle$, and $|\uparrow\rangle \equiv |D_{5/2}, m_j = -3/2\rangle$, where m_j is the projection of the angular momentum along the quantisation axis defined by a static magnetic field ≈ 0.5 mT. We calibrate the phase of the initial $\pi/2$ pulse for Alice's atom, relative to ϕ, to remain in the optimal entangled state for measuring Δ_- (see Supplementary Information § B). The data required for comparison of the three measurement methods, at a given Ramsey duration, is taken in a single experiment sequence as shown in Fig. 1b. We use the data from the unentan-

gled state to obtain both the single-ion and the two-ion parity signals. The dominant source of decoherence in this experiment is fluctuation of the qubit transition frequency due to magnetic field noise. To suppress this decoherence and enable longer Ramsey durations, we use active magnetic field stabilisation and a modified spin-echo sequence (see Supplementary Information § C).

We perform Ramsey experiments with durations from 0.1 ms to 20 ms for both the entangled and unentangled states. Figure 2 shows a comparison of these experiments at 0.1 ms and 17.5 ms. To measure the oscillation only from the term in Eq. 3 containing Δ_-, we set $\phi_2 = -\phi_1$ and scan ϕ_1. At $T_R = 0.1$ ms, we observe a slight reduction in contrast for the unentangled ions, mainly due to imperfect spin-echo pulses; imperfect entanglement fidelity further reduces the contrast for the entangled state. At longer durations, qubit decoherence due to magnetic field noise reduces the contrast of all the parity signals (see Fig. S2). The sensitivity of the single-ion signal to laser phase noise is evident from the additional reduction in the contrast. When the laser phase noise at the fibre output was intentionally increased by turning off the FNC, we observed high contrast for the two-ion signals at probe durations where the single-ion signals had decohered completely (see Fig. S6). This demonstrates a decoherence-free subspace encoded in two qubits separated by a macroscopic distance. In principle, our network could also be used to enhance measurements of Δ_+, which is required to stabilise the laser frequency to the mean atomic frequency. However, the entangled state needed for this measurement has an increased sensitivity to laser dephasing (see Fig. S3), hence accessing this enhancement will require improvements in laser technology.

To illustrate the enhancement from the entangled state for frequency comparisons, we plot the single-shot uncertainty for the single-ion and two-ion measurements versus the Ramsey duration (see Fig. 3a). As expected from Eq. 2, the single-shot measurement uncertainty decreases with T_R until, at longer durations, it rises due to reduction in the parity contrast. We note that the majority of the measurements have a higher uncertainty compared to ideal single-ion measurements limited only by quantum projection noise (dashed curve). We observe the advantage of probing two ions simultaneously at longer Ramsey durations, where the uncertainty for the single-ion measurements increases due to laser dephasing. At all durations, the entangled state yields the lowest experimental uncertainty, with a minimum at $T_R = 10$ ms.

We define the entanglement enhancement as the ratio of the number of measurements required to reach a given precision σ without entanglement ($N_{s|u}$), to the number of measurements required using the entangled state (N_e), where σ is given by

$$\sigma = \frac{\delta\Delta_{-,s|u|e}}{\sqrt{N_{s|u|e}}}. \tag{4}$$

Thus, the entanglement enhancement is equivalent to $N_{s|u}/N_e = (\delta\Delta_{-,s|u}/\delta\Delta_{-,e})^2$, where s, u, and e correspond to measurements with single ions, unentangled ions, or entangled ions, respectively. In Fig. 3b we plot this entanglement enhancement versus the Ramsey duration. Relative to the single-ion measurements, we observe an enhancement which is initially close to the expected factor of 2, but increases at longer durations. In this regime, correlated measurements using two unentangled ions have a reduced uncertainty com-

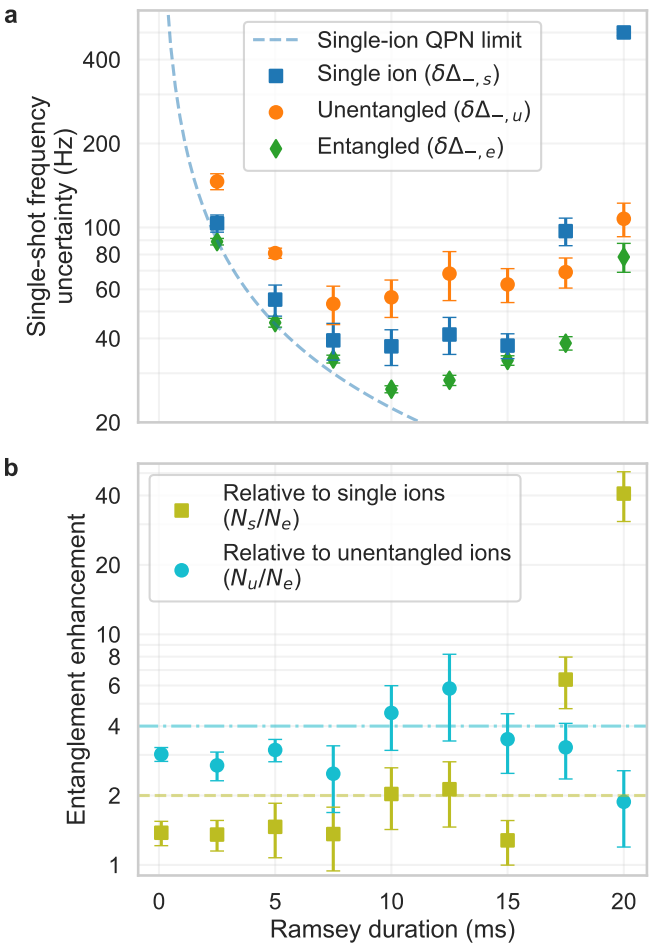

FIG. 3: **Characterisation of entanglement enhancement.** **a**, Single-shot frequency uncertainties for single-ion ($\delta\Delta_{-,s}$), correlated unentangled ($\delta\Delta_{-,u}$), and entangled ($\delta\Delta_{-,e}$) measurements, versus Ramsey duration (T_R), excluding other contributions to the experimental duty cycle. The blue dashed line indicates the minimum uncertainty achievable by single-ion measurements limited only by quantum projection noise (QPN), i.e. single-ion measurements with perfect contrast. The data at $T_R = 0.1$ ms are omitted for clarity. At all durations, the entangled state achieves the lowest single-shot uncertainty. At longer durations, the single-ion measurements have the highest uncertainty due to their sensitivity to laser dephasing. **b**, Entanglement enhancement versus Ramsey duration (T_R) relative to single-ion measurements (olive squares) and relative to measurements with two unentangled ions (turquoise circles), where $N_{s|u}/N_e = (\delta\Delta_{-,s|u}/\delta\Delta_{-,e})^2$. The theoretical enhancements are 2 relative to the single-ion (olive dashed line) and 4 relative to the unentangled state (turquoise dash-dotted line). All error bars indicate 68% confidence intervals.

pared to the single-ion measurements. Entanglement yields an even greater enhancement: we observe close to a factor of 4 enhancement relative to the unentangled state at all durations.

Finally, as a proof of principle, we use entanglement to enhance the measurement precision of an applied frequency difference between the two ions. This frequency difference arises from an AC Stark shift due to a far-detuned 674 nm beam which illuminates Alice's ion throughout the Ramsey duration (here 15 ms). As shown in Fig. 4a, when the AC Stark shift is applied we see about a factor 2 increase in the signal for the entangled state as compared to the unentangled state. From the parity response, we measure a frequency difference Δ_- of -8.8 ± 2.5 Hz with the unentangled state, and -8.6 ± 0.6 Hz with the entangled state (see Fig. 4b), a fractional frequency uncertainty of $\sim 10^{-15}$. The measurement uncertainty without entanglement is higher than the expected factor of 2 compared to the measurement with entanglement. This is likely due to an increased uncertainty in the parity signal for the unentangled state due to the term corresponding to P_+ in Eq. 3, which contributes excess noise to the measurement at this Ramsey duration even though the mean offset has averaged to zero (see Supplementary Information § J). This results in an above-statistical scatter in the unentangled measurements, as can be seen in Fig. 4a. Probing the atoms at a duration much longer than the timescale for laser dephasing would remove this noise.

In conclusion, we have demonstrated enhanced frequency comparisons using an elementary quantum network of two entangled trapped-ion atomic clocks. The high fidelity and speed of entanglement generation in our network, which give a large signal and an efficient duty cycle, show that entangled clocks can potentially offer a practical enhancement for metrology. Compared to probe durations of ∼500 ms used in state-of-the-art optical clocks[2], our mean entanglement generation duration of 9 ms would have a negligible effect on the measurement duty cycle. We were restricted to the use of short probe durations (compared to the limit set by the $^{88}Sr^+$ $4D_{5/2}$ lifetime[49] of ≈ 400 ms) by qubit decoherence due to magnetic field fluctuations. The magnetic field fluctuations could be reduced significantly through the use of superconducting solenoids[50], mu-metal shielding[51], or more advanced dynamical decoupling schemes[52]. While our demonstration used single $^{88}Sr^+$ ions, whose simple level structure enables fast entanglement generation, the remote entanglement could in principle be mapped to any ion species via quantum logic operations[53], with negligible loss of fidelity or speed[54]. For example, we could choose an ion with a transition that has a reduced magnetic field sensitivity[1], a narrower linewidth, or an increased sensitivity to fundamental constants[7]. The stability of the entangled state phase ϕ would be an important consideration for attaining state-of-the-art measurement precisions. Increasing the distance between nodes is important for remote sensing and geodesy. Longer fibres with phase noise cancellation[55] could be used at the cost of a reduced entanglement rate due to fibre losses at 422 nm; downconversion to telecom wavelengths[56] could reduce losses. Using local operations to increase the number of entangled ions in each node could further reduce the measurement uncertainty

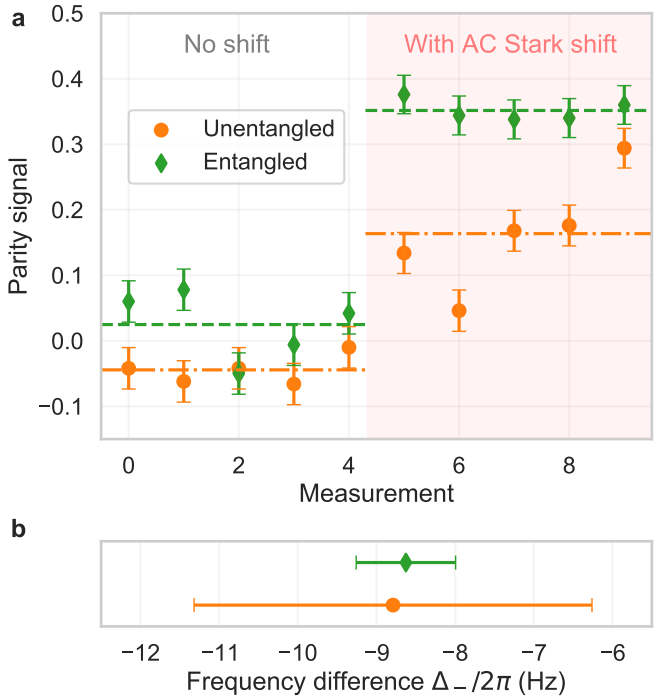

FIG. 4: **Measurement of clock-clock frequency difference with and without entanglement. a,** We plot the two-ion parity signal with (green diamonds) and without (orange circles) entanglement at a Ramsey duration of 15 ms, choosing the analysis phase ϕ_1 to sit at the steepest slope of the parity signal (see Fig. S8). The average parity signal with and without the shift are shown for the entangled (green dashed line) and unentangled state (orange dash-dotted line). The first five points are without any frequency shift, the next five points (shaded area) are with a shift applied to Alice's ion. The change in parity signal for the entangled state is about twice as large as for the unentangled states. Error bars indicate 68% confidence intervals, given by quantum projection noise. **b**, Measured frequency difference with and without entanglement. From the change in the parity signal measured in **a**, we determine frequency differences of -8.6 ± 0.6 Hz and -8.8 ± 2.5 Hz, with and without entanglement, respectively. Error bars indicate 68% confidence intervals.

for frequency comparisons. In principle, an entangled clock network with additional nodes connected via photonic links could also improve measurements of a common frequency reference[23]; however, such an implementation would not have the common-mode phase suppression achieved here for atom-atom frequency comparisons. Our demonstration provides the first building block towards such a network that could operate beyond the SQL, at the fundamental Heisenberg limit.

Acknowledgements: We thank E.R. Clements, R.M. Godun, D.B. Hume, and A.M. Steane for helpful discussions and insightful comments on the manuscript. We would like to thank Sandia National Laboratories for supplying the HOA2 ion

traps used in these experiments. **Funding:** This work was supported by the UK EPSRC Hub in Quantum Computing and Simulation (EP/T001062/1), the E.U. Quantum Technology Flagship Project AQTION (No. 820495), and C.J.B.'s UKRI Fellowship (MR/S03238X/1). B.C.N. acknowledges funding from the UK National Physical Laboratory. **Author contributions:** D.P.N., B.C.N., P.D., D.M., G.A., R.S., and C.J.B. built and maintained the experimental apparatus; R.S. conceived the experiments; B.C.N. and R.S. carried out the experiments, assisted by D.P.N., P.D., D.M., and G.A.; B.C.N., R.S., and D.M.L. analyzed the data; B.C.N. and R.S. wrote the manuscript with input from all authors; C.J.B. and D.M.L. secured funding and supervised the work. **Competing interests:** C.J.B. is a director of Oxford Ionics. The remaining authors declare no competing interests. **Data availability:** Source data for all plots are available. All other data or analysis code that support the plots are available from the corresponding authors upon reasonable request.

SUPPLEMENTARY INFORMATION

A. Mapping remote entanglement to optical qubit

The initial entanglement is generated using the $|S_{1/2}, m_J = \pm 1/2\rangle$ states that are separated by 14 MHz[19]. To generate this entaglement, we first excite both atoms simultaneously to the $|P_{1/2}, m_J = +1/2\rangle$ state using a fast pulse from a 422 nm picosecond laser. The spontaneously emitted 422 nm photons, whose polarisations are entangled with the internal state of the ions, are collected in single-mode optical fibres. The fibres transmit these photons to a Bell-state analyser, where measurements conditioned on the photon polarisations project the ions into an entangled state. To map this entanglement to the optical qubit on each atom, we use a π-pulse on the $|S_{1/2}, m_J = +1/2\rangle \leftrightarrow |D_{5/2}, m_J = -3/2\rangle$ transition. This sequence creates the entangled Bell state

$$|\Psi\rangle = \frac{1}{\sqrt{2}}(|\downarrow\uparrow\rangle \pm e^{i\phi}|\uparrow\downarrow\rangle), \tag{S1}$$

where $|\downarrow\rangle \equiv |S_{1/2}, m_j = -1/2\rangle$, and $|\uparrow\rangle \equiv |D_{5/2}, m_j = -3/2\rangle$.

B. Bell-state phase calibration

We measure the frequency difference between the atoms $\Delta_- = \Delta_1 - \Delta_2 = \omega_2 - \omega_1$, where $\Delta_i = \omega_L - \omega_i$. The laser and atomic frequencies are denoted by ω_L and ω_i respectively. To measure Δ_- using entangled atoms, we require the state $|\Psi\rangle = \frac{1}{\sqrt{2}}(|\downarrow\uparrow\rangle \pm e^{i\phi}|\uparrow\downarrow\rangle)$. Entanglement can also improve measurements of $\Delta_+ = \Delta_1 + \Delta_2$, which can be used to stabilise the laser frequency to the mean atomic frequency; this measurement requires the entangled state $|\Phi\rangle = \frac{1}{\sqrt{2}}(|\downarrow\downarrow\rangle \pm e^{i\phi'}|\uparrow\uparrow\rangle)$.

We initially create the entangled state $|\Psi\rangle = \frac{1}{\sqrt{2}}(|\downarrow\uparrow\rangle \pm e^{i\phi}|\uparrow\downarrow\rangle)$, where ϕ is set by optical paths in the apparatus, and $\pm$ corresponds to the specific detector pattern in the Bell state analyser that heralds entanglement[19]. To remain in the optimal entangled state for measuring Δ_-, we adjust the phase of the Ramsey experiment (ϕ_0 in Fig 1b) in Alice with respect to that in Bob to be $\phi_0 = \phi + \pi$. Sample calibration data is shown in Fig. S1, where we determine the optimal ϕ_0 required for each of the 4 possible valid detector patterns. This phase is updated in real time within the experimental sequence to acquire data from all heralds. Figure S2 shows the parity contrast versus time for the single-ion measurements, the two-ion unentangled state and the two-ion entangled state $|\Psi\rangle$. By setting $\phi_0 = \phi$, we can transform $|\Psi\rangle$ to $|\Phi\rangle$. We also performed Ramsey experiments using $|\Phi\rangle$ as shown in Fig. S3. As $|\Phi\rangle$ is symmetric, we set $\phi_2 = \phi_1$ and scanned ϕ_1 for these data. This state has a faster decay in contrast due to increased sensitivity to laser dephasing.

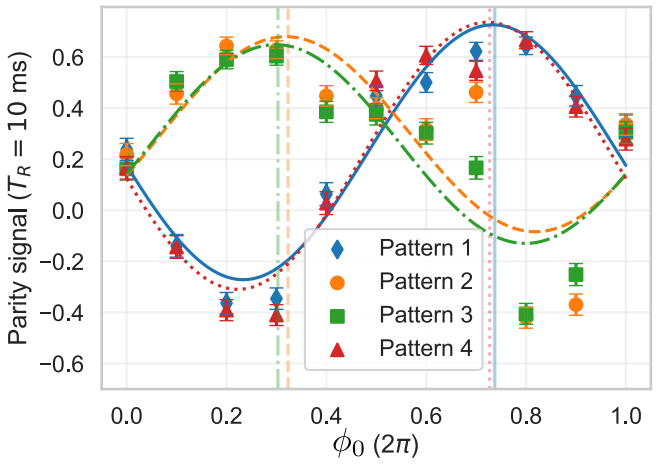

FIG. S1: Calibration of ϕ_0, the relative phase of the Ramsey experiments in Alice with respect to Bob. For a Ramsey duration of 10 ms, and fixed analysis phases ϕ_1 and ϕ_2, we plot the two-ion parity versus ϕ_0 for each of the 4 detector patterns in the Bell state analyser[19]. The optimal ϕ_0 corresponds to the peak of the parity signal (vertical lines). Patterns 1 (blue diamonds) and 4 (red triangles) are approximately π radians out of phase from patterns 2 (orange circles) and 3 (green squares), corresponding to the phase offset of the resulting entangled state.

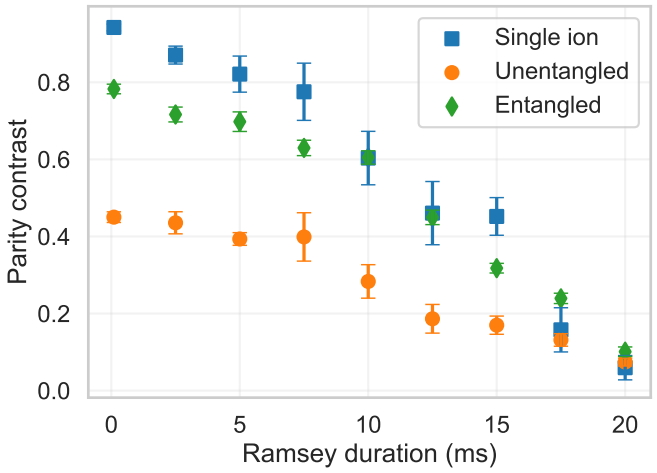

FIG. S2: Parity contrast versus Ramsey duration. For each Ramsey duration, we perform phase scans as shown in Fig. 2 and measure the contrast. The single-ion measurements are the average contrast from Alice and Bob. For single-ion (blue squares), unentangled (orange circles), and entangled (green diamonds) measurements, the contrast decays due to qubit decoherence. The contrast for the single-ion measurements also decays due to laser dephasing.

C. Echo sequence

We alternate between the optical transitions $|\downarrow\rangle \equiv |S_{1/2}, m_j = -1/2\rangle \leftrightarrow |\uparrow\rangle \equiv |D_{5/2}, m_j = -3/2\rangle$ and

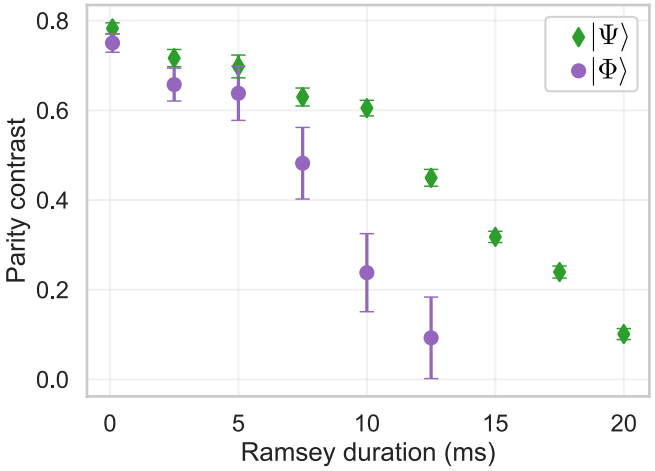

FIG. S3: Two-ion parity contrast versus Ramsey duration for $|\Psi\rangle = \frac{1}{\sqrt{2}}(|{\downarrow\uparrow}\rangle \pm e^{i\phi}|{\uparrow\downarrow}\rangle)$ and $|\Phi\rangle = \frac{1}{\sqrt{2}}(|{\downarrow\downarrow}\rangle \pm e^{i\phi'}|{\uparrow\uparrow}\rangle)$. Compared to $|\Psi\rangle$ (green diamonds), $|\Phi\rangle$ (purple circles) has a faster decay in contrast due to an increased sensitivity to laser dephasing. All error bars indicate 68% confidence intervals.

$|\downarrow'\rangle \equiv |S_{1/2}, m_j = +1/2\rangle \leftrightarrow |\uparrow'\rangle \equiv |D_{5/2}, m_j = +3/2\rangle$, which have magnetic field sensitivities of -11.2 MHz/mT and $+11.2$ MHz/mT, respectively. Thus, by alternating between these transitions, we can 'echo out' slow qubit frequency drifts due to fluctuations in the magnetic field, while still measuring a shift of the centre-of-gravity of the 674 nm transition. To map $|\uparrow\rangle \to |\uparrow'\rangle$ and $|\downarrow\rangle \to |\downarrow'\rangle$, we perform the following echo sequence using 674 nm π-pulses resonant with the required transition, as illustrated in Fig. S4:

1. $|\uparrow\rangle \equiv |D_{5/2}, m_j = -3/2\rangle \to |S_{1/2}, m_j = +1/2\rangle$
2. $|S_{1/2}, m_j = +1/2\rangle \to |D_{5/2}, m_j = +3/2\rangle \equiv |\uparrow'\rangle$
3. $|\downarrow\rangle \equiv |S_{1/2}, m_j = -1/2\rangle \to |D_{5/2}, m_j = -3/2\rangle$
4. $|D_{5/2}, m_j = -3/2\rangle \to |S_{1/2}, m_j = +1/2\rangle \equiv |\downarrow'\rangle$

The total duration of this pulse sequence is $\approx 44\,\mu$s. To map $|\downarrow'\rangle \to |\downarrow\rangle$ and $|\uparrow'\rangle \to |\uparrow\rangle$, we perform the same sequence in reverse order. For the experiments described in the main text, we perform a total of 5 such sequences to achieve Walsh-7 modulation[57]. The Ramsey duration T_R excludes the length of these echo sequences. The choice of Walsh sequence index depends on the magnetic field noise spectrum; for our system, the Walsh-7 sequence optimally increased the coherence time without significantly reducing the contrast due to imperfect π-pulses, as shown in Fig. S5. For single qubit-rotations, we observe an error of $\sim 5 \times 10^{-4}$. This error increases to $\sim 3 \times 10^{-3}$ for the entangled state due to heating of the ions during the entanglement-attempt sequence.

D. Magnetic field stabilisation

The two primary sources of magnetic-field noise are fluctuations in the current supplied to the coils, and ambient AC fields at 50 Hz (and harmonics) induced by wires carrying mains current in the vicinity of the traps. Stabilisation circuits[58] on the magnetic field coils reduce these noise sources and increase the coherence time of the optical $^{88}Sr^+$ qubit from 0.75(1) ms to 7.1(1) ms.

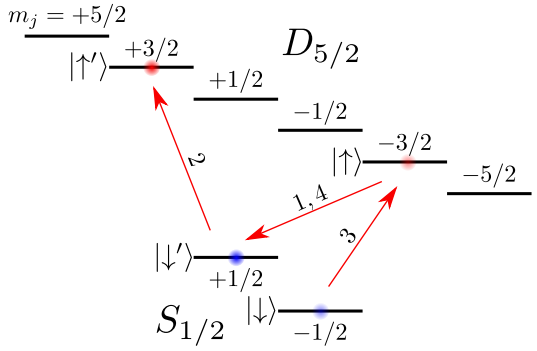

FIG. S4: Modified spin-echo sequence. We map the $|\downarrow\rangle$ and $|\uparrow\rangle$ qubit states to the $|\downarrow'\rangle$ and $|\uparrow'\rangle$ states following the pulse sequence described in the text. The primed states have equal and opposite magnetic field sensitivities to the unprimed states.

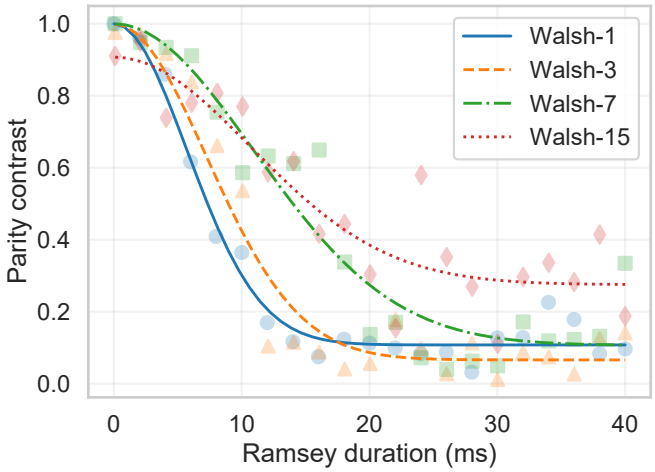

FIG. S5: Single-ion parity contrast versus Ramsey duration for different Walsh sequence indices 1 (blue circles), 3 (orange triangles), 7 (green squares), and 15 (red diamonds). As we increase the Walsh sequence index, we observe higher contrasts at longer durations. We fit a Gaussian decay to each dataset. For the experiments described in the main text, we use a Walsh-7 sequence.

E. Fibre noise cancellation

The fibre noise cancellation (FNC) for the 674 nm light uses an acousto-optical modulator (AOM) before the 15 m fibre to the optical table with Alice and Bob. We pick off light before this AOM, which is superimposed on a photodiode with light retro-reflected from the output facet of the fibre. We use this error signal to modify the rf input to the AOM[59]. All the

experiments described in the main text were performed with this FNC turned on. The two-ion correlated measurements are insensitive to laser dephasing, as discussed in the text. While this is visible at long Ramsey durations, additional decoherence from magnetic field fluctuations further decreases the parity contrast. To unambiguously demonstrate the insensitivity to laser dephasing, we performed additional experiments with the FNC turned off, as shown in Fig. S6. Compared to the data in Fig. 2, at $T_R = 2.5$ ms we observe a complete loss in contrast of the single-ion signals due to laser dephasing, while the two-ion signals are essentially unchanged.

F. Duration of entanglement generation

We simultaneously excite each ion using a 422 nm pulse, and the spontaneously emitted photons are transmitted to the Bell state analyser where a coincident detection of a pair of photons projects the ions into an entangled state. As we only detect a small fraction of the emitted photons, the entanglement generation is probabilistic and has a variable duration. We note that, because the entanglement is heralded, all events are used without any post-selection. Each attempt has a duration of 1 μs, with 250 μs of laser cooling after every 1000 attempts. For the data in this work, the mean entanglement generation duration is about 9 ms. We plot the histogram of entanglement generation durations for a sample dataset in Fig. S7.

G. Single-ion and two-ion parity signal calculations

At the readout stage of the experimental sequence, we determine whether each ion was in the $|\downarrow\rangle$ or $|\uparrow\rangle$ state by recording its fluorescence. An ion in the state $|\downarrow\rangle$ is bright, while an ion in the $|\uparrow\rangle$ state is dark. For multiple repetitions at a given Ramsey duration, we can then determine the probability of each ion being in $|\downarrow\rangle$ ($P_\downarrow$) or $|\uparrow\rangle$ ($P_\uparrow$). The expectation value is $\langle\hat{\sigma}_{zi}\rangle = P_\uparrow - P_\downarrow = 1 - 2P_\downarrow$. To determine the parity for the two-ion measurements, we calculate $\langle\hat{\Pi}\rangle = \langle\hat{\sigma}_{z1}\hat{\sigma}_{z2}\rangle$. We use the same data to calculate the single-ion and the correlated unentangled two-ion parity signals using unentangled ions.

H. Entanglement-enhancement calculation

As given in Eq. 2, the single-shot frequency uncertainty for measuring $\Delta_i = \omega_L - \omega_i$ from a parity scan is

$$\delta\Delta_i = \frac{\delta\langle\hat{\Pi}_i\rangle}{C_i T_R},$$

where T_R is the Ramsey wait duration, C_i is the contrast of the single-ion parity fringe, and $\delta\langle\hat{\Pi}_i\rangle$ is the parity measurement uncertainty, which is ideally limited only by projection noise[39] and hence has a value of 1. From the single-ion experiments, the single-shot uncertainty in Δ_- is therefore

$$\delta\Delta_{-,s} = \frac{\delta\langle\hat{\Pi}_i\rangle}{T_R}\sqrt{\frac{1}{C_1^2}+\frac{1}{C_2^2}}. \tag{S2}$$

For the correlated two-ion measurements, the single-shot uncertainty in Δ_- is given by

$$\delta\Delta_{-,u|e} = \frac{\delta\langle\hat{\Pi}\rangle}{C T_R},$$

where C is now the contrast of the two-ion parity fringe. For $C_1 = C_2 = C$, using an entangled state thus gives a $\sqrt{2}$ reduction in the measurement uncertainty compared to single-atom measurements. Using simultaneous measurements of an unentangled two-ion state, C has a maximum value of $\frac{1}{2}$, which increases the single-shot uncertainty by a factor of 2 compared to the entangled state.

For Fig. 3, to obtain an error bar for the single-shot uncertainties and the entanglement enhancement, we only consider the uncertainty in the fitted parity contrasts and propagate the error accordingly.

I. Calibration for Stark shift measurement

To generate a differential shift between the two ions, we illuminate Alice's ion with a detuned 674 nm beam during the 15 ms Ramsey wait duration which gives an AC Stark shift. This beam is 35 MHz red-detuned from the $|S_{1/2}, m_j = -1/2\rangle \leftrightarrow |D_{5/2}, m_j = -3/2\rangle$ transition and has a power of $\sim 20\,\mu$W. The calibration data for the frequency shift measurement in Fig. 4 is shown in Fig. S8. The fitted Ramsey fringes allow us to convert a change in the parity signal to a frequency shift.

J. Effect of laser dephasing on parity signal

For the two-ion parity data in Fig. S2, we plot the error in the fitted contrasts and the value of the y-offset for the unentangled ions in Fig. S9. For the data in Fig. 4, we chose a Ramsey duration of 15 ms. At this duration, the y-offset was close to zero, but there was still some contribution to the fitted contrast error due to laser dephasing. However, at longer durations the overall contrast for both the entangled and unentangled ions had decayed further due to qubit frequency fluctuations.

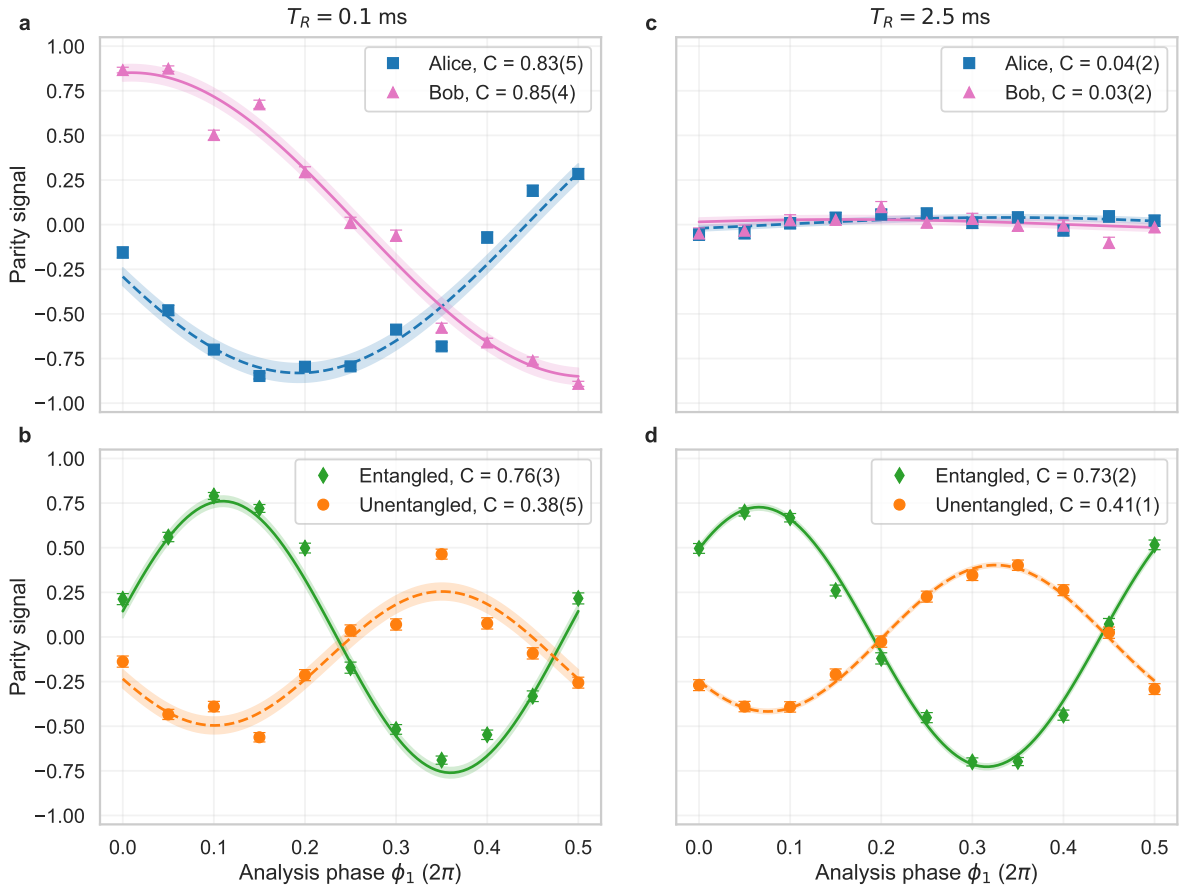

FIG. S6: Comparison of parity fringes with fibre noise cancellation (FNC) turned off, with and without entanglement, at Ramsey durations of 0.1 ms and 2.5 ms. We scan the analysis phase $\phi_1 = -\phi_2$ from 0 to π. We plot the single-ion data for each of Alice (blue squares) and Bob (pink triangles), and the two-ion data with (green diamonds) and without (orange circles) entanglement. (a) and (b) correspond to a Ramsey duration of 0.1 ms, while (c) and (d) correspond to a Ramsey duration of 2.5 ms. At 2.5 ms, qubit decoherence is minimal; the decoherence of the single-ion signals is primarily from laser dephasing, whilst the two-ion signals show no decrease in contrast. The shaded regions show the 68% confidence intervals of the best fit lines.

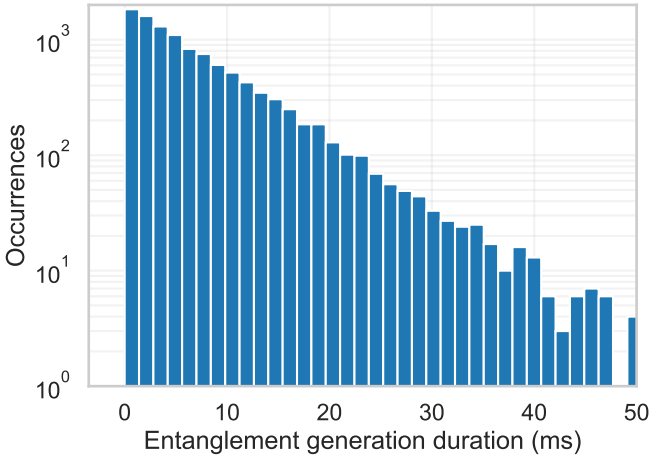

FIG. S7: Histogram of entanglement generation durations for a sample dataset. A total of 11000 attempts are plotted, with a mean duration of 9.2 ms.

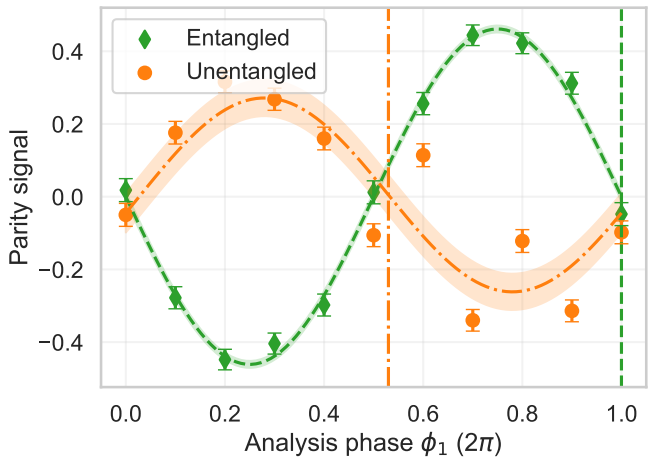

FIG. S8: Calibration data for the frequency difference measurement in Fig. 4a. For these data, $\phi_2 = 0$ and we only scan the value of ϕ_1 from 0 to 2π radians with no shift applied. From these data, we choose the phases at the steepest slopes indicated by the vertical lines for the unentangled (orange dash-dotted) and entangled (green dashed) states, respectively. The shaded regions indicate the 68% confidence intervals. As in Fig. 4a, the above-statistical scatter of the unentangled data points is evident.

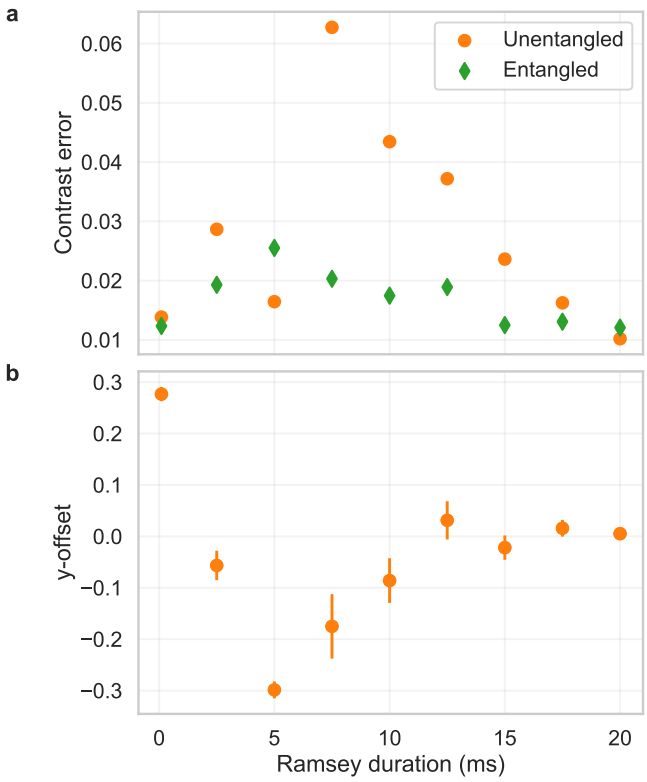

FIG. S9: Details of two-ion parity data from Fig. S2 for unentangled and entangled ions. a, For each value of the Ramsey duration, we plot the the error in the fitted value of contrast, C, from the parity signal for the two-ion data with (green diamonds) and without (orange circles) entanglement. Laser dephasing contributes to the error for the unentangled two-ion signal through the P_+ term (see Eq. 3), which is not present for the entangled-state parity. We suspect that this error increases because the Ramsey duration is similar to the timescale of the laser dephasing, which increases the uncertainty of the contrast due to the P_+ term. At longer durations, contributions from this term are reduced, and the magnitude of the error for the unentangled and entangled two-ion signals is similar at 20 ms. b, The parity signal for the unentangled two-ion signal is fitted with a y-offset to account for the P_+ term. We plot the value of this offset for all Ramsey durations. The y-offset reaches zero before the contributions of this term to the error have fully decayed.

[1] Brewer, S. M. *et al.* $^{27}Al^{+}$ Quantum-Logic Clock with a Systematic Uncertainty below 10^{-18}. *Phys. Rev. Lett.* **123**, 033201 (2019).

[2] Oelker, E. *et al.* Demonstration of 4.8×10^{-17} stability at 1 s for two independent optical clocks. *Nat. Photonics* **13**, 714–719 (2019).

[3] Ludlow, A. D., Boyd, M. M., Ye, J., Peik, E. & Schmidt, P. O. Optical atomic clocks. *Rev. Mod. Phys.* **87**, 637 (2015).

[4] Rosenband, T. *et al.* Frequency ratio of Al^{+} and Hg^{+} Single-Ion Optical Clocks; Metrology at the 17th Decimal Place. *Science* **319**, 1808–1812 (2008).

[5] Lange, R. *et al.* Improved limits for violations of local position invariance from atomic clock comparisons. *Phys. Rev. Lett.* **126**, 011102 (2021).

[6] Derevianko, A. & Pospelov, M. Hunting for topological dark matter with atomic clocks. *Nat. Phys.* **10**, 933–936 (2014).

[7] Safronova, M. S. *et al.* Search for new physics with atoms and molecules. *Rev. Mod. Phys.* **90**, 025008 (2018).

[8] Chou, C.-W., Hume, D. B., Rosenband, T. & Wineland, D. J. Optical clocks and relativity. *Science* **329**, 1630–1633 (2010).

[9] Mehlstäubler, T. E., Grosche, G., Lisdat, C., Schmidt, P. O. & Denker, H. Atomic clocks for geodesy. *Rep. Prog. Phys.* **81**, 064401 (2018).

[10] McGrew, W. *et al.* Atomic clock performance enabling geodesy below the centimetre level. *Nature* **564**, 87–90 (2018).

[11] Meyer, V. *et al.* Experimental Demonstration of Entanglement-Enhanced Rotation Angle Estimation Using Trapped Ions. *Phys. Rev. Lett.* **86**, 5870–5873 (2001).

[12] Leibfried, D. *et al.* Toward Heisenberg-Limited Spectroscopy with Multiparticle Entangled States. *Science* **304**, 1476–1478 (2004).

[13] Roos, C. F., Chwalla, M., Kim, K., Riebe, M. & Blatt, R. 'Designer atoms' for quantum metrology. *Nature* **443**, 316–319 (2006).

[14] Megidish, E., Broz, J., Greene, N. & Häffner, H. Improved Test of Local Lorentz Invariance from a Deterministic Preparation of Entangled States. *Phys. Rev. Lett.* **122**, 123605 (2019).

[15] Manovitz, T., Shaniv, R., Shapira, Y., Ozeri, R. & Akerman, N. Precision Measurement of Atomic Isotope Shifts Using a Two-Isotope Entangled State. *Phys. Rev. Lett.* **123**, 203001 (2019).

[16] Pedrozo-Peñafiel, E. *et al.* Entanglement on an optical atomic-clock transition. *Nature* **588**, 414–418 (2020).

[17] Moehring, D. L. *et al.* Entanglement of single-atom quantum bits at a distance. *Nature* **449**, 68–71 (2007).

[18] Monroe, C. *et al.* Large-scale modular quantum-computer architecture with atomic memory and photonic interconnects. *Phys. Rev. A* **89**, 022317 (2014).

[19] Stephenson, L. J. *et al.* High-Rate, High-Fidelity Entanglement of Qubits Across an Elementary Quantum Network. *Phys. Rev. Lett.* **124**, 110501 (2020).

[20] Clements, E. R. *et al.* Lifetime-Limited Interrogation of Two Independent $^{27}Al^{+}$ Clocks Using Correlation Spectroscopy. *Phys. Rev. Lett.* **125**, 243602 (2020).

[21] Hume, D. B. & Leibrandt, D. R. Probing beyond the laser coherence time in optical clock comparisons. *Phys. Rev. A* **93**, 032138 (2016).

[22] Kim, M. E. *et al.* Optical coherence between atomic species at the second scale: improved clock comparisons via differential spectroscopy. *arXiv:2109.09540* (2021).

[23] Komar, P. *et al.* A quantum network of clocks. *Nat. Phys.* **10**, 582–587 (2014).

[24] Wineland, D. J., Bollinger, J. J., Itano, W. M., Moore, F. & Heinzen, D. J. Spin squeezing and reduced quantum noise in spectroscopy. *Phys. Rev. A* **46**, R6797 (1992).

[25] Wineland, D. J., Bollinger, J. J., Itano, W. M. & Heinzen, D. Squeezed atomic states and projection noise in spectroscopy. *Phys. Rev. A* **50**, 67 (1994).

[26] Degen, C. L., Reinhard, F. & Cappellaro, P. Quantum sensing. *Rev. Mod. Phys.* **89**, 035002 (2017).

[27] Pezzè, L., Smerzi, A., Oberthaler, M. K., Schmied, R. & Treutlein, P. Quantum metrology with nonclassical states of atomic ensembles. *Rev. Mod. Phys.* **90**, 035005 (2018).

[28] Caves, C. M. Quantum-mechanical noise in an interferometer. *Phys. Rev. D* **23**, 1693 (1981).

[29] Tse, M. *et al.* Quantum-Enhanced Advanced LIGO Detectors in the Era of Gravitational-Wave Astronomy. *Phys. Rev. Lett.* **123**, 231107 (2019).

[30] Malnou, M. *et al.* Squeezed Vacuum Used to Accelerate the Search for a Weak Classical Signal. *Phys. Rev. X* **9**, 021023 (2019).

[31] Wolf, F. *et al.* Motional Fock states for quantum-enhanced amplitude and phase measurements with trapped ions. *Nat. Commun.* **10**, 1–8 (2019).

[32] Gilmore, K. A. *et al.* Quantum-enhanced sensing of displacements and electric fields with two-dimensional trapped-ion crystals. *Science* **373**, 673–678 (2021).

[33] Kimble, H. J. The quantum internet. *Nature* **453**, 1023–1030 (2008).

[34] Gisin, N., Ribordy, G., Tittel, W. & Zbinden, H. Quantum cryptography. *Rev. Mod. Phys.* **74**, 145–195 (2002).

[35] Monroe, C. & Kim, J. Scaling the ion trap quantum processor. *Science* **339**, 1164–1169 (2013).

[36] Hensen, B. *et al.* Loophole-free Bell inequality violation using electron spins separated by 1.3 kilometres. *Nature* **526**, 682–686 (2015).

[37] Ramsey, N. F. A Molecular Beam Resonance Method with Separated Oscillating Fields. *Phys. Rev.* **78**, 695–699 (1950).

[38] Ramsey, N. F. Resonance experiments in successive oscillatory fields. *Rev. Sci. Instrum.* **28**, 57–58 (1957).

[39] Itano, W. M. *et al.* Quantum projection noise: Population fluctuations in two-level systems. *Phys. Rev. A* **47**, 3554 (1993).

[40] Giovannetti, V., Lloyd, S. & Maccone, L. Quantum Metrology. *Phys. Rev. Lett.* **96**, 010401 (2006).

[41] Riis, E. & Sinclair, A. G. Optimum measurement strategies for trapped ion optical frequency standards. *J. Phys. B* **37**, 4719–4732 (2004).

[42] Leroux, I. D. *et al.* On-line estimation of local oscillator noise and optimisation of servo parameters in atomic clocks. *Metrologia* **54**, 307–321 (2017).

[43] Bize, S. *et al.* Interrogation oscillator noise rejection in the comparison of atomic fountains. *IEEE Trans. Ultrason. Ferroelectr. Freq. Control* **47**, 1253–1255 (2000).

[44] Chwalla, M. *et al.* Precision spectroscopy with two correlated atoms. *Appl. Phys. B* **89**, 483–488 (2007).

[45] Marti, G. E. *et al.* Imaging Optical Frequencies with 100 μHz Precision and 1.1 μm Resolution. *Phys. Rev. Lett.* **120**, 103201 (2018).

[46] Young, A. W. *et al.* Half-minute-scale atomic coherence and high relative stability in a tweezer clock. *Nature* **588**, 408–413 (2020).

[47] Nadlinger, D. P. *et al.* Device-Independent Quantum Key Distribution. *arXiv:2109.14600* (2021).

[48] Stephenson, L. *Entanglement between nodes of a quantum network*. Ph.D. thesis, University of Oxford (2019).

[49] Sahoo, B. K., Islam, M. R., Das, B. P., Chaudhuri, R. K. & Mukherjee, D. Lifetimes of the metastable $^2D_{3/2,5/2}$ states in Ca^+, Sr^+, and Ba^+. *Phys. Rev. A* **74**, 062504 (2006).

[50] Gabrielse, G. & Tan, J. Self-shielding superconducting solenoid systems. *J. Appl. Phys* **63**, 5143–5148 (1988).

[51] Ruster, T. *et al.* A long-lived Zeeman trapped-ion qubit. *Appl. Phys. B* **122** (2016).

[52] Aharon, N., Spethmann, N., Leroux, I. D., Schmidt, P. O. & Retzker, A. Robust optical clock transitions in trapped ions using dynamical decoupling. *New J. Phys.* **21**, 083040 (2019).

[53] Schmidt, P. O. *et al.* Spectroscopy using quantum logic. *Science* **309**, 749–752 (2005).

[54] Hughes, A. C. *et al.* Benchmarking a High-Fidelity Mixed-Species Entangling Gate. *Phys. Rev. Lett.* **125**, 080504 (2020).

[55] Boulder Atomic Clock Optical Network (BACON) Collaboration. Frequency ratio measurements at 18-digit accuracy using an optical clock network. *Nature* **591**, 564–569 (2021).

[56] Wright, T. A. *et al.* Two-way photonic interface for linking the Sr^+ transition at 422 nm to the telecommunication C band. *Phys. Rev. App.* **10**, 044012 (2018).

[57] Harmuth, H. F. Applications of Walsh functions in communications. *IEEE Spectr.* **6**, 82–91 (1969).

[58] Merkel, B. *et al.* Magnetic field stabilization system for atomic physics experiments. *Rev. Sci. Instrum.* **90**, 044702 (2019).

[59] Thirumalai, K. *High-fidelity mixed species entanglement of trapped ions*. Ph.D. thesis, University of Oxford (2019).